PHYSICAL REVIEW B **95**, 161402(R) (2017)

Short-range atomic ordering in nonequilibrium silicon-germanium-tin semiconductors

S. Mukherjee,[1] N. Kodali,[1] D. Isheim,[2] S. Wirths,[3] J. M. Hartmann,[4] D. Buca,[3] D. N. Seidman,[2] and O. Moutanabbir[1,*]

[1]*Department of Engineering Physics, École Polytechnique de Montréal, Montréal, C.P. 6079, Succ. Centre-Ville, Montréal, Québec, Canada H3C 3A7*

[2]*Department of Materials Science and Engineering and Northwestern University Center for Atom-Probe Tomography, Northwestern University, Evanston, Illinois 60208-3108, USA*

[3]*Peter Grünberg Institute 9 and JARA-FIT, Forschungszentrum Juelich, Juelich 52425, Germany*

[4]*CEA, LETI, Minatec Campus, 17 rue des Martyrs, Grenoble 38054, France*

(Received 5 October 2016; revised manuscript received 4 January 2017; published 10 April 2017)

The precise knowledge of the atomic order in monocrystalline alloys is fundamental to understand and predict their physical properties. With this perspective, we utilized laser-assisted atom probe tomography to investigate the three-dimensional distribution of atoms in nonequilibrium epitaxial Sn-rich group-IV SiGeSn ternary semiconductors. Different atom probe statistical analysis tools including frequency distribution analysis, partial radial distribution functions, and nearest-neighbor analysis were employed in order to evaluate and compare the behavior of the three elements to their spatial distributions in an ideal solid solution. This atomistic-level analysis provided clear evidence of an unexpected repulsive interaction between Sn and Si leading to the deviation of Si atoms from the theoretical random distribution. This departure from an ideal solid solution is supported by first-principles calculations and attributed to the tendency of the system to reduce its mixing enthalpy throughout the layer-by-layer growth process.

DOI: 10.1103/PhysRevB.95.161402

The assumption that the arrangement of atoms within the crystal lattice is perfectly random is a broadly used approximation to establish the physical properties of semiconductor alloys. This approximation allows one to estimate rather accurately certain thermodynamic as well as material parameters such as the excess enthalpy of formation, Vegard-like lattice parameters, and band gaps that are smaller than the composition weighted average (optical bowing). However, it has been proposed that some ternary semiconductors can deviate from this assumed perfect solid solution. Indeed, both calculations and experiments suggested the presence of local atomic order in certain III-V alloys [1–8]. This phenomenon manifests itself when at least one of the elements forming the alloy preferentially occupies or avoids specific lattice sites. This induces short-range order in the lattice with an impact on the basic properties of the alloyed semiconductors [3–7].

The recent progress in developing Sn-rich group-IV (SiGeSn) ternary semiconductors and their integration in a variety of low-dimensional systems and devices have revived the interest in elucidating the atomistic-level properties of monocrystalline alloys [9–20]. Interestingly, unlike III-V semiconductors, achieving a direct band gap in $Si_xGe_{1-x-y}Sn_y$ requires a sizable incorporation of Sn (>10 at. %), which is significantly higher than the equilibrium solubility (<1 at. %). Understanding the atomic structure of these metastable alloys is therefore imperative for implementing predictive models to describe their basic properties. With this perspective, we present a study of the atomic order in $Si_xGe_{1-x-y}Sn_y$ alloys (x and y in the $0.04 - 0.19$ and $0.02 - 0.12$ range, respectively). We employed atom probe tomography (APT) which allows atomistic-level investigations [21–24] and statistical tools to analyze the three-dimensional (3D) distributions of the three elements. This analysis unraveled an unexpected repulsive interaction between Sn and Si leading to a deviation of Si atoms from the theoretical random distribution.

The samples investigated in this work were grown using a metal cold-wall reduced pressure chemical vapor deposition [10,25,26] using Si_2H_6, Ge_2H_6, and $SnCl_4$ as precursors and a relatively low growth temperature of 350–475 °C resulting in a normal growth rate of ~1 nm/s. Further details of epitaxial growth of $Si_xGe_{1-x-y}Sn_y$ layers are described in the Supplemental Material [27]. Figure 1(a) shows the scanning transmission electron microscope (STEM) images of the layer with highest Sn content ($Si_{0.04}Ge_{0.84}Sn_{0.12}$), confirming the pseudomorphic growth of the ternary layers without dislocations or extended defects. Figure 1(b) shows the corresponding 3D APT reconstructed map. The details of APT analysis along with data sets recorded from different layers are given in the Supplemental Material [27]. For cluster analysis, isoconcentration surfaces were first defined at varying Sn and Si concentrations within the reconstructed maps. No evidence of any aggregates was found, regardless of the content. The mass spectra of Si, Ge, and Sn, displaying all the isotopes and the evaporated charge states are shown in Fig. S2 of the Supplemental Material [27]. In order to investigate the short-range atomic distribution, we performed a series of statistical analyses, namely, the frequency distribution (FD) analysis, the partial radial distribution function (p-RDF) analysis, and the nearest-neighbor (NN) analysis within predefined regions in 3D maps. The theoretical formalism of each method is outlined in the Supplemental Material [27]. Figure 2(a) displays the FD of Si, Ge, and Sn in $Si_{0.04}Ge_{0.84}Sn_{0.12}$. The coefficient of determination (R^2) between the observed value (y_i) and the binomial distribution (f_i) was calculated from the residual sum of squares $S_{res} = \sum_i (y_i - f_i)^2$ and the total sum of squares $S_{tot} = \sum_i (y_i - \bar{y})^2$, and the relation $R^2 = 1 - \frac{S_{res}}{S_{tot}}$ with $\bar{y} = \frac{1}{n}\sum_{i=1}^{n} y_i$. The figure shows the mean values of the experimental FD for Si, Ge, and Sn correspond to 4.0, 84.0, and 12.0 at. %, respectively. This agrees with

*Corresponding author: oussama.moutanabbir@polymtl.ca

 ©2017 American Physical Society

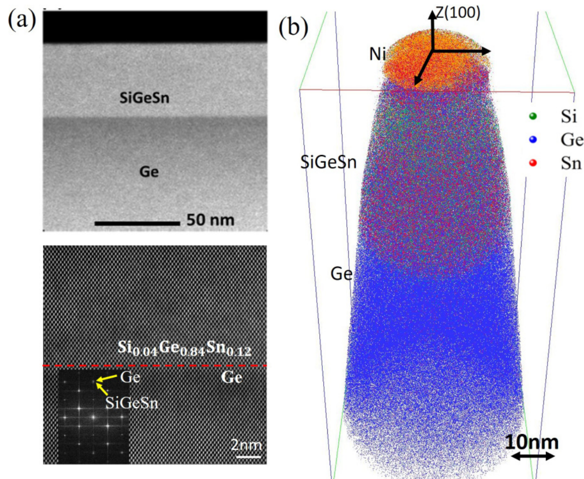

FIG. 1. (a) High-angle annular dark field STEM (top) and high-resolution STEM (bottom) images of the $Si_{0.04}Ge_{0.84}Sn_{0.12}$/Ge interface. Inset: A diffraction pattern taken from a selected region at the interface. (b) 3D reconstruction of the ternary alloy ($Si_{0.04}Ge_{0.84}Sn_{0.12}$), showing the Ni capping layer, the SiGeSn thin film, and a portion of the Ge buffer layer. For the sake of clarity, only 10% of Ge atoms and 50% of Sn atoms are displayed

the concentrations found in the proximity histogram in Fig. S1(a) of the Supplemental Material [27]. Additionally, it reveals that while Ge and Sn closely follow the binomial distribution (calculated R^2 for Ge and Sn are 0.9999 and 0.9978, respectively), Si shows a small disagreement with binomial distribution (calculated R^2 for Si is 0.9679). We eliminate statistical fluctuations as a possible reason for this observed deviation because the probed volume is large enough to have a significant number of Si atoms. In Fig. 2(b), we show the p-RDF of Sn and Si in $Si_{0.04}Ge_{0.84}Sn_{0.12}$ with respect to Sn, Ge, and Si. It is worthwhile to state that in all analyses carried out for different layers, Ge is always found to be random. Henceforth, we shall restrict our discussion mainly to the behavior of Si and Sn. Also noteworthy is the fact that p-RDF is meaningful only for $r \geqslant 0.5$ nm. For $r < 0.5$ nm, the APT data analysis program does not find any atom and generates random values for p-RDF. The p-RDFs in all the plots for $r < 0.5$ nm have been shaded. The following facts are evident from Fig. 2(b): Si shows a negative correlation with respect to Sn and a positive correlation with respect to Ge as well as itself; Sn has its p-RDF at unity with respect to Ge and Si, while it shows signs of a positive correlation with respect to itself. The p-RDFs of Sn and Si with respect to Sn in the top panel in Fig. 2(b) show a puzzling behavior. First, Sn is seen to have a positive correlation with itself. However, the FD and the NN distribution (later in Fig. 4) do not give any indication that Sn deviates from a perfect random distribution. Second, the p-RDFs do not converge to unity at large values of r, unlike that in the lower two panels in Fig. 2(b). We think that this unexpected behavior might be due to minute long-range compositional variations of Sn across the reconstructed APT maps.

The observations in Fig. 2 provide clear evidence that Si atoms are disrupted from a perfect random distribution. The negative correlation shown by Si with respect to Sn hints at the presence of a repulsive interaction between the

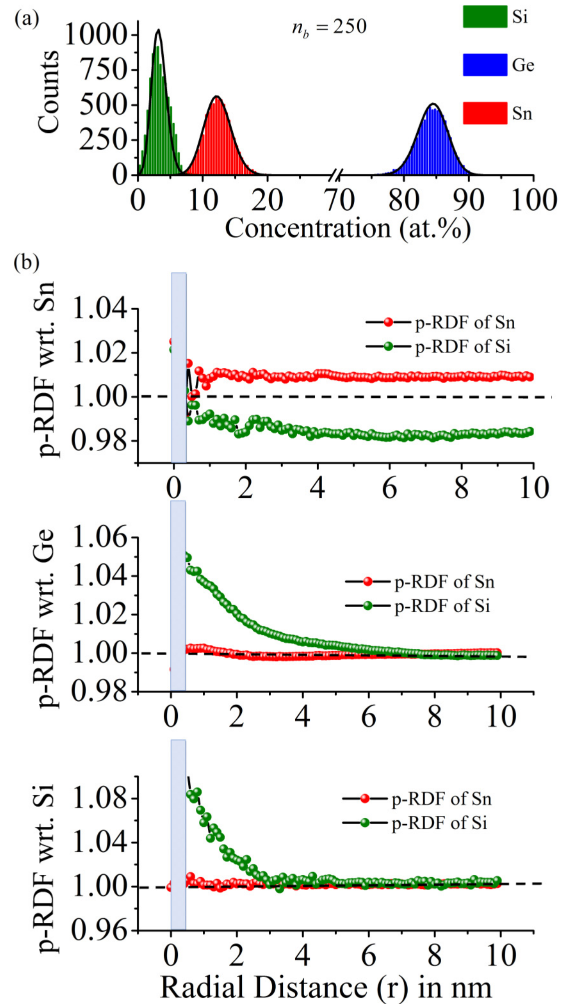

FIG. 2. (a) Frequency distribution of Si (green), Ge (blue), and Sn (red) in $Si_{0.04}Ge_{0.84}Sn_{0.12}$ as determined from APT reconstruction (in histograms). The corresponding binomial distributions of these atoms are shown in black continuous lines. (b) The partial radial distribution function of Sn and Si atoms with respect to Sn (top), Ge (middle), and Si (bottom) in the same sample as in (a) for $r = 10$ nm. The Integrated Visualization and Analysis Software (IVAS) computed error bars are smaller than the data symbols. The black dotted line represents p-RDF = 1.

two species. This phenomenon provides new insights into the growth kinetics of metastable alloys by chemical vapor deposition [25], where the growth conditions prevent Sn atoms from forming equilibrium aggregated phase, despite the fact that the growth of a complete monolayer takes place in ∼0.1 s, which is a very slow process compared to the time scale of surface diffusion events. The data presented in Fig. 2 suggest that the repulsive interaction between Si and Sn results from these elements diffusing away from each other during the growth, justifying the negative correlation of Si with respect to Sn. Note that the p-RDFs are plotted relative to each other and normalized to the bulk concentration of an element. The repulsive interaction should have a subtle effect on the distribution of Sn and Ge as well, but the p-RDFs of Sn and Ge when plotted with respect to Si do not reflect this behavior due to their higher concentrations with respect to Si. The Si

atoms diffusing away from Sn can either hop to other Ge atoms or make a large number of hops to other Si atoms (which are scarce). Hence, we see a positive correlation of Si with respect to Ge and also with respect to itself. Since bulk diffusion is energetically less favorable than surface diffusion, it is reasonable to conclude that the observed departure for an ideal solid solution occurs during the layer-by-layer growth. It is important to note that this phenomenon is peculiar to Sn-rich ternary alloys since extended x-ray absorption fine-structure (EXAFS) investigations indicated the atomic distribution in Sn-rich strained and relaxed GeSn binary alloys to be random [28], also asserting the fact that epitaxial strain is not responsible for the observation we made in Fig. 2.

Interestingly, the analysis of ternary layers with lower Sn contents ($\leqslant$4 at. %) indicates that the aforementioned departure from a perfectly random alloy is either absent or too small to be detected. For instance, Fig. 3(a) exhibits the FD for each element in $Si_{0.10}Ge_{0.875}Sn_{0.025}$. Noteworthy is the overlap between the observed distribution and the binomial distribution (black lines) assuming a complete random alloy (R^2 was calculated for Si, Ge, and Sn to be 0.9989, 0.9999, and 0.9959, respectively). Figure 3(b) shows the measured Sn and Si p-RDF within a sphere of radius 10 nm. Here, the p-RDF of Sn with respect to Sn shows the telltale signature of statistical fluctuations owing to its small concentration of only 2.5 at. %. The p-RDF fluctuates around the mean value of unity and the magnitude of these fluctuations decreases with increasing r. Note that the volume of the shell considered during p-RDF analysis and consequently the number of atoms which lie inside the shell increases as a function of r^2. Finally, the p-RDF of Sn steadies down to the value of unity. The p-RDFs of Si with respect to Si and Sn are qualitatively similar, none showing any noticeable deviation from 1. The p-RDF of Sn with respect to Si, Ge and Si with respect to Ge, shown in Fig. S3 of the Supplemental Material [27], confirm that at low Sn content, all atoms are randomly distributed within the alloy, reinforcing the results of the FD analysis.

Figure 4(a) displays the analysis of NN distribution $NN_{A\text{-}A}\text{-}k$, where A is Si or Sn; k is 2 (second NN), 3 (third NN), and 5 (fifth NN) for $Si_{0.04}Ge_{0.84}Sn_{0.12}$. Figure 4(b) shows the departure of the observed NN distribution from the theoretical value, $P_k(r,C)$. The NN-1, 4, 10 distribution for Si and Sn and their corresponding departure from $P_k(r,C)$ in $Si_{0.04}Ge_{0.84}Sn_{0.12}$ is shown in Fig. S4 of the Supplemental Material [27]. Figures 4 and S4 show that while $NN_{Sn\text{-}Sn}$ follow the probability distribution closely, $NN_{Si\text{-}Si}$ does not. A shoulder starts to develop at a lower value of r than the maxima of $P_k(r,C)$ in the observed $NN_{Si\text{-}Si}$ distribution, which gets more prominent with increasing k. The rest of the measured $NN_{Si\text{-}Si}$ distribution shows a minute right shift relative to $P_k(r,C)$. These observed departures are clear indications of a disruption in Si distribution creating local pockets where there are more Si with respect to a given Si atom. In these pockets, the Si concentration is slightly higher than the average bulk concentration making the average distance between the NNs slightly smaller than what is expected theoretically. The minute right shift also indicates that the rest of the matrix is slightly depleted of Si making the NN distances slightly larger than that in a perfect random distribution. The

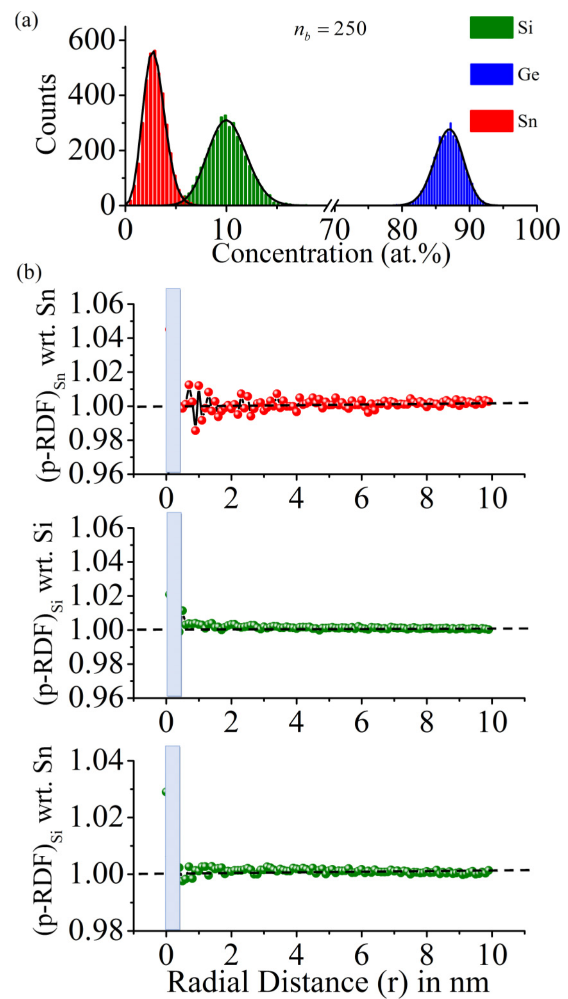

FIG. 3. (a) Frequency distribution of Si (green), Ge (blue), and Sn (red) in $Si_{0.10}Ge_{0.875}Sn_{0.025}$ as determined from APT reconstruction (in histograms). The corresponding binomial distributions of these atoms are shown in black continuous lines. (b) The partial radial distribution function in the same sample as (a) for $r = 10$ nm of Sn atoms with respect to Sn (top), Si with respect to Si (middle), and Si with respect to Sn (bottom). The IVAS computed error bars are smaller than the data symbols. The black dotted line represents p-RDF = 1.

shoulder is obviously absent in $NN_{Si\text{-}Si}$-1 [Fig. S4(a)] due to the fact that no atom can be located at a distance smaller than the first-nearest-neighbor distance. Also noteworthy is the fact that such features are absent in the NN distributions within the alloy with low Sn content of 2.5 at. % (see Fig. S5 of the Supplemental Material [27]). The deviation shown by $NN_{Sn\text{-}Sn}$ in Fig. S5(b) is purely random in nature owing to its small concentration, in contrast with the deviation shown by $NN_{Si\text{-}Si}$ in Fig. 4(b) [a +ve deviation below the maxima of $P_k(r,C)$, a −ve deviation at the maxima of $P_k(r,C)$, followed by a small +ve deviation above the maxima of $P_k(r,C)$]. It must, however, be remembered that the observed deviation of Si in Sn-rich alloys from a perfect random atomic distribution must not be confused with the formation of aggregates [29,30].

The revelation that Si atoms in monocrystalline Sn-rich ternary alloys deviate from the behavior in an ideal solid solution is indeed surprising. We attributed this disruption

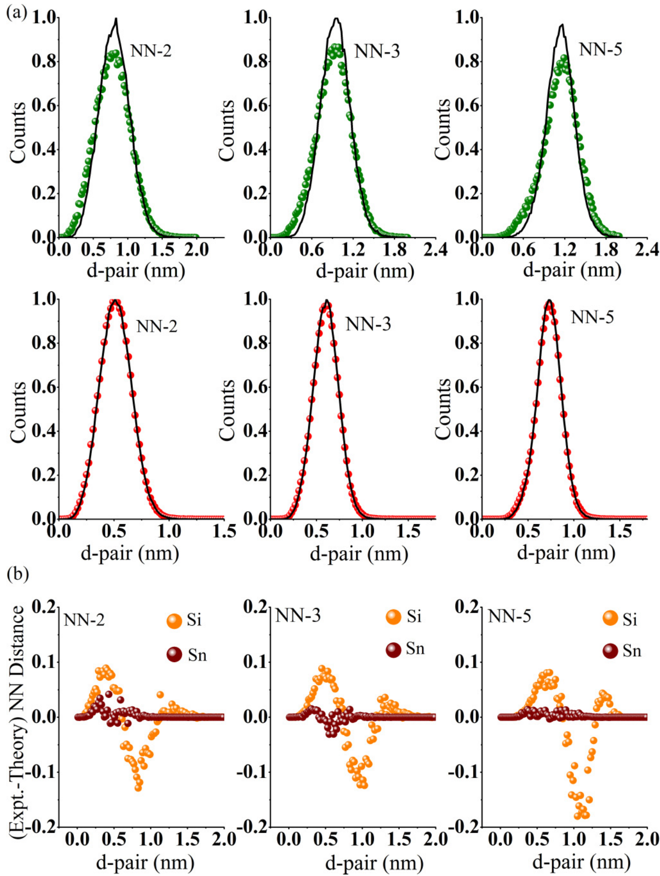

FIG. 4. (a) Si-Si and Sn-Sn NN-2, -3, and -5 distribution in the alloy containing 12.0 at. % Sn. The distributions as determined from APT reconstruction are shown in solid spheres: Si (green) and Sn (red). The corresponding binomial distributions are shown in black continuous lines. All the data sets are normalized with respect to the theoretical probability distribution, $P_k(r,C)$. (b) Departure of the observed Si-Si and Sn-Sn NN-2, -3, and -5 distributions from the binomial distribution. The y axes in all three figures are the same.

in Si distribution to a repulsive interaction between the Sn and Si atoms. In order to elucidate the energetics of this phenomenon, we performed detailed density functional theory (DFT) calculations using the QUANTUM ESPRESSO code (details are provided in the Supplemental Material [27]) on a 32-atom supercell. As shown in Fig. S7 of the Supplemental Material [27], we found that a Si-Sn bond is indeed energetically not favorable requiring an additional energy of $\sim+50-250$ meV/unit cell as compared to the most stable configurations (NN-3 and NN-4). A similar observation was made during a recent EXAFS study on SiGeSn ternary alloys [31]. These calculations support qualitatively the hypothesized repulsive interaction between Si and Sn atoms. Here, it is important to notice that the incorporation of a large radius Sn atom in Ge lattice would create a local distortion leading to more compressive Ge regions around Sn. This seems to affect the incorporation of Si, which has a smaller radius, and perhaps prefers to incorporate in available sites far from these compressive regions. What we must remember, however, is that the growth of a metastable alloy is a kinetically controlled nonequilibrium process. Owing to limited mobility, atoms after deposition on the surface are inhibited to reach the equilibrium state within the growth time scale. The problem therefore reduces to a surface process where one needs to evaluate how atoms behave at the surface before they become buried underneath the next growing layer. Herein, one can reasonably neglect bulk diffusion as it implies energy barriers that are significantly higher than those for surface diffusion. One can also intuitively assume that, once atoms are deposited on a surface, the system will begin to evolve to minimize the mixing enthalpy ΔH_{mix} in an effort to reduce its Gibbs free energy. This evolution is abruptly brought to an end after the next growing layer sweeps across the entire surface. Since Ge is the solvent and Si and Sn are solutes, the mixing enthalpy ΔH_{mix} is given by $\Delta H_{\mathrm{mix}} = H_{\mathrm{alloy}} - xH_{\mathrm{Si}} - (1-x-y)H_{\mathrm{Ge}} - yH_{\mathrm{Sn}}$. With the mole fractions and the enthalpies of the pure elements (H_{Si}, H_{Ge}, H_{Sn}) predetermined, H_{alloy} becomes a determining parameter. H_{alloy} is affected by factors such as epitaxial strain, microstrain, and chemical interaction. Microstrain arises when the lattice has to accommodate two atoms of dissimilar size yet maintain a uniform lattice constant throughout the crystal. For example, with N the total number of atoms and $\Omega_{\mathrm{Si\text{-}Sn}}$ the Si-Sn interaction parameter, the microstrain contribution coming from Si-Sn bonds in a regular solution is given by $N\Omega_{\mathrm{Si\text{-}Sn}}(xy)$. Unlike the epitaxial strain and microstrain whose contribution to H_{alloy} is always positive, the chemical interaction contribution (ΔH_{Ch}) to H_{alloy} can be positive or negative. This depends on the nature of charge transfer between two atoms forming a bond. For example, calculations showed that in ordered $\mathrm{GaInP_2}$ the difference in electronegativity between the atoms caused charge to flow from the less ionic Ga-P bond to the more ionic In-P, giving a small positive value of ΔH_{Ch} [1]. The process of charge transfer takes place not only for bonding atoms which belong to different groups (hence different electronegativity) but also for isovalent heteropolar atoms such as group-IV elements. Indeed, first-principles calculations found a small positive and a small negative value of ΔH_{Ch} for SiGe and SiC, respectively [32].

In summary, we performed atomic scale studies on Sn-rich metastable SiGeSn ternary alloys using APT. To investigate the randomness in the distribution of different atoms within the alloys, we implemented different statistical techniques, namely, the FD, p-RDFs, and the NN distribution. Our study shows that the Si atoms deviate from a perfectly random solid solution within the alloy with large Sn content. The phenomenon is attributed to a repulsive interaction between Sn and Si, thereby inducing local disruptions in an otherwise random distribution of Si. The DFT calculations also demonstrated that having Si and Sn atoms as nearest neighbors is indeed energetically unfavorable. These departures from an ideal solid solution shown by Si is either absent or too weak to be detected in alloys with low Sn content (<4 at. %). The observed short-range ordering must be taken into account for a more accurate evaluation of lattice parameters, lattice relaxation, thermodynamic parameters, band structure, and optoelectronic properties of group-IV ternary semiconductors.

The work was supported by NSERC-Canada (Discovery Grant: RGPIN421837-12; Strategic Partnership Grant: STPGP 494031), Canada Research Chair (Award No. 950-228250), Calcul Québec, and Compute Canada. The LEAP at the

Northwestern University Center for Atom-Probe Tomography (NUCAPT) was acquired and upgraded with equipment grants from the MRI program of the National Science Foundation (Grant No. DMR-0420532) and the DURIP program of the Office of Naval Research (Grants No. N00014-0400798, No. N00014-0610539, and No. N00014-0910781). NUCAPT is supported by the NSF's MRSEC program (Grant No. DMR-1121262). Additional instrumentation at NUCAPT was supported by the Initiative for Sustainability and Energy at Northwestern (ISEN).

[1] G. P. Srivastava, J. L. Martins, and A. Zunger, Phys. Rev. B **31**, 2561 (1985).
[2] M. Ichimura and A. Sasaki, J. Appl. Phys. **60**, 3850 (1986).
[3] A. Mascarenhas, S. Kurtz, A. Kibbler, and J. M. Olson, Phys. Rev. Lett. **63**, 2108 (1989).
[4] T. Kanata, M. Nishimoto, H. Nakayama, and T. Nishino, Phys. Rev. B **45**, 6637 (1992).
[5] D. C. Meyer, K. Richter, P. Paufler, and G. Wagner, Phys. Rev. B **59**, 15253 (1999).
[6] L. Alagna, T. Prosperi, S. Turchini, C. Ferrari, L. Francesio, and P. Franzosi, J. Appl. Phys. **83**, 3552 (1998).
[7] C. Bocchi, P. Franzosi, and C. Ghezzi, J. Appl. Phys. **57**, 4533 (1985).
[8] T. S. Kuan, T. F. Kuech, W. I. Wang, and E. L. Wilkie, Phys. Rev. Lett. **54**, 201 (1985).
[9] A. Attiaoui and O. Moutanabbir, J. Appl. Phys. **116**, 063712 (2014).
[10] S. Wirths, A. T. Tiedemann, Z. Ikonic, P. Harrison, B. Holländer, T. Stoica, G. Mussler, M. Myronov, J. M. Hartmann, D. Grützmacher, D. Buca, and S. Mantl, Appl. Phys. Lett. **102**, 192103 (2013).
[11] G. Sun, H. H. Cheng, J. Menéndez, J. B. Khurgin, and R. A. Soref, Appl. Phys. Lett. **90**, 251105 (2007).
[12] J. D. Gallagher, C. Xu, L. Jiang, J. Kouvetakis, and J. Menéndez, Appl. Phys. Lett. **103**, 202104 (2013).
[13] J. Kouvetakis, J. Menendez, and A. V. G. Chizmeshya, Annu. Rev. Mater. Res. **36**, 497 (2006).
[14] P. Moontragoon, R. A. Soref, and Z. Ikonic, J. Appl. Phys. **112**, 073106 (2012).
[15] K. Lu Low, Y. Yang, G. Han, W. Fan, and Y.-C. Yeo, J. Appl. Phys. **112**, 103715 (2012).
[16] S. Gupta, B. Magyari-Köpe, Y. Nishi, and K. C. Saraswat, J. Appl. Phys. **113**, 073707 (2013).
[17] R. Kotlyar, U. E. Avci, S. Cea, R. Rios, T. D. Linton, K. J. Kuhn, and I. A. Young, Appl. Phys. Lett. **102**, 113106 (2013).
[18] M. Oehme, D. Widmann, K. Kostecki, P. Zaumseil, B. Schwartz, M. Gollhofer, R. Koerner, S. Bechler, M. Kittler, E. Kasper, and J. Schulze, Opt. Lett. **39**, 4711 (2014).
[19] S. Takeuchi, A. Sakai, K. Yamamoto, O. Nakatsuka, M. Ogawa, and S. Zaima, Semicond. Sci. Technol. **22**, S231 (2007).
[20] R. Chen, S. Gupta, Y.-C. Huang, Y. Huo, C. W. Rudy, E. Sanchez, Y. Kim, T. I. Kamins, K. C. Saraswat, and J. S. Harris, Nano Lett. **14**, 37 (2014).
[21] S. Mukherjee, H. Watanabe, D. Isheim, D. N. Seidman, and O. Moutanabbir, Nano Lett. **16**, 1335 (2016).
[22] E. P. Silaeva, L. Arnoldi, M. L. Karahka, B. Deconihout, A. Menand, H. J. Kreuzer, and A. Vella, Nano Lett. **14**, 6066 (2014).
[23] D. E. Perea, I. Arslan, J. Liu, Z. Ristanović, L. Kovarik, B. W. Arey, J. A. Lercher, S. R. Bare, and B. M. Weckhuysen, Nat. Commun. **6**, 7589 (2015).
[24] W. Chen, L. Yu, S. Misra, Z. Fan, P. Pareige, G. Patriarche, S. Bouchoule, and P. R. I. Cabarrocas, Nat. Commun. **5**, 4134 (2014).
[25] J.-H. Fournier-Lupien, S. Mukherjee, S. Wirths, E. Pippel, N. Hayazawa, G. Mussler, J. M. Hartmann, P. Desjardins, D. Buca, and O. Moutanabbir, Appl. Phys. Lett. **103**, 263103 (2013).
[26] S. Wirths, D. Buca, and S. Mantl, Prog. Cryst. Growth Charact. Mater. **62**, 1 (2016).
[27] See Supplemental Material at http://link.aps.org/supplemental/10.1103/PhysRevB.95.161402 for details of epitaxial gowth of the alloys and the atom probe investigation, the theoretical background of the statistical tools, additional results concenring the statistical analysis on the atom probe data set, and the DFT calculations.
[28] F. Gencarelli, D. Grandjean, Y. Shimura, B. Vincent, D. Banerjee, A. Vantomme, W. Vandervorst, R. Loo, M. Heyns, and K. Temst, J. Appl. Phys. **117**, 095702 (2015).
[29] R. K. W. Marceau, L. T. Stephenson, C. R. Hutchinson, and S. P. Ringer, Ultramicroscopy **111**, 738 (2011).
[30] F. De Geuser, W. Lefebvre, and D. Blavette, Philos. Mag. Lett. **86**, 227 (2006).
[31] Y. Shimura, T. Asano, T. Yamaha, M. Fukuda, W. Takeuchi, O. Nakatsuka, and S. Zaima, Mater. Sci. Semicond. Process (2016), doi:10.1016/j.mssp.2016.11.013.
[32] J. L. Martins and A. Zunger, Phys. Rev. Lett. **56**, 1400 (1986).